Novel Molecular Doping Mechanism for n-doping of SnO_2 via Triphenylphosphine Oxide and Its Effect on Perovskite Solar Cells

Bao Tu,[a,b†] Yangfan Shao,[b,c†] Wei Chen,[a,d†] Yinghui Wu, [a] Xin Li,[e] Yanling He,[c] Jiaxing Li,[c] Fangzhou Liu,[d] Zheng Zhang,[a] Yi Lin,[a] Xiaoqi Lan,[a] Leiming Xu,[a] Xingqiang Shi,[c] Alan Manching Ng,[c] Haifeng Li,[b]* Lungwa Chung,[e] Aleksandra B. Djurišić,[d] Zhubing He [a]*

[a] Department of Materials Science and Engineering, Shenzhen Key Laboratory of Full Spectral Solar Electricity Generation (FSSEG), Southern University of Science and Technology, No. 1088, Xueyuan Rd., Shenzhen, 518055, Guangdong, China.

[b] Institute of Applied Physics and Materials Engineering, University of Macau, Macau SAR, China

[c] Department of Physics, Southern University of Science and Technology, No. 1088, Xueyuan Rd., Shenzhen, 518055, Guangdong, China.

[d] Department of Physics, The University of Hong Kong, Pokfulam, Hong Kong SAR, China.

[e] Department of Chemistry, Southern University of Science and Technology, No. 1088, Xueyuan Rd., Shenzhen, 518055, Guangdong, China.

† All the three authors contributed equally to this work.

E-mail: hezb@sustc.edu.cn; haifengli@umac.mo

Abstract

Molecular doping of inorganic semiconductor is a rising topic in the scope of organic/inorganic hybrid electronics. However, it is difficult to find dopant molecules which simultaneously exhibit strong reducibility and stability in ambient atmosphere, which are needed for *n*-type doping of oxide semiconductors. In this work, we demonstrate successful *n*-type doping of SnO_2 by a simple, air-robust and cost-effective triphenylphosphine oxide molecule. Strikingly, we discovered that electrons were transferred from the R_3P^+-O^- σ-bond to the peripheral tin atoms other than the directly interacted ones at the surface. That means those electrons are delocalized. The course was verified by multi physical characterizations. This doping effect accounts for the enhancement of conductivity and the decline of work function of SnO_2, which enlarges the built-in field from 0.01 eV to 0.07 eV and decreases the energy barrier from 0.55 eV to 0.39 eV at the SnO_2/Perovskite interface enabling an increase in the conversion efficiency of perovskite solar cells from 19.01% to 20.69%.

Introduction

Doping is a general way to modulate the electronic structure of materials to improve their based device performance. Ionic doping is widely used in inorganic semiconductors to increase conductivity by increasing the carrier density of majority carriers.[1] However, this process can result in increased disorder and defects in the crystal lattice, resulting in the degradation of carrier mobility and parasitic recombination. Ideally, a doped semiconductor should have both high conductivity and high charge carrier mobility. Different doping strategies have been used in organic materials, which typically contain large molecules and can have amorphous structure or small grain size and large number of imperfections or impurities compared to epitaxially grown inorganic semiconductors.[2] In contrast with inorganic material doping where dopant acts as a point defect in the crystal lattice, in organic molecules two processes can occur: formation of host and dopant ion pairs, and the formation of ground state charge transfer complexes. [3, 4] While the organic systems offer excellent tunability by varying the chemical structure of host and dopant molecules, the doping efficiency needs to be improved.

One possible strategy to address the different problems existing in doped inorganic and organic materials is to develop hybrid organic-inorganic systems which would combine the advantages of both types from materials. When an organic molecule is adsorbed on the surface of an inorganic nanocrystal, charge transfer from the organic molecule to the inorganic semiconductor can occur, without inducing defects within the inorganic semiconductor. Consequently, this approach was successfully applied to the surface doping of some inorganic nanocrystals by organic molecules in recent years.[5-12] In 2014, Rietwyk et al. reported firstly this novel doping mechanism of electrons transferring from the absorbed molecular donor (methylcoboltocene) to the silicon surface.[5] Tarasov et al. employed air stable dihydrobenzimidazole derivatives (2-Fc-DMBI-H) and benzimidazoline radicals ((2-Fc-DMBI)$_2$) to obtain effective n-type doping of MoS_2 few-layer nanosheets.[6] Kirmani et al. successfully realized the electronic structure modulation of PbS

quantum dots via molecular doping of some p and n type metal-organic chelates dopants.[7] The new doping method has shown increasing impact on the academic research community of optoelectronics and energy.[9, 12]

More recently, our group demonstrated a successful surface molecular doping of NiO nanoscrystals by 2,2′-(perfluoronaphthalene-2,6-diylidene)dimalononitrile (F6TCNNQ) for high performance perovskite solar cells (PSCs), where it is verified by multi-photophysical tools of electrons transfer from already *p*-type NiO nanocrystals film to F6TCNNQ due to stronger electron capture ability of fluorine atoms in the air stable F6TCNNQ molecules compared to the oxygen atoms in NiO nanocrystals.[13] This results in higher hole concentration without detrimental effects on the of mobility in the NiO nanocrystals film, which improves the performance of PSCs. This good result moves us further to strengthen electronic properties of SnO_2 nanocrystals film by surface molecular doping, which acts already as another promising material for electron transport in PSCs.[14-18] However, compared with *p*-type molecular doping, successful *n*-type doping of inorganic semiconductors is more difficult.[6, 7, 9] So far, only some limited kinds of expensive, unstable and complex chelate molecules were involved as electron donors for *n*-type molecular doping of inorganic semiconductors.[5-7, 9-11] This problem is mainly due to the scarcity of molecules which simultaneously exhibit both strong reducibility and stability simultaneously in ambient atmosphere. Moreover, simple and robust molecular structure as well as cost-effectiveness are also requirements in the evolution of this promising technique.

On the other hand, various surface modification of SnO_2 were successfully employed to enhance electrons transfer at the cathode side and hence to improve the device performances.[19-27] These enhancements were mainly attributed to the passivation of surface trap states of SnO_2 film and antisite defects of perovskites, dipole effect and band level alignment adjustments. In this work, a simple, air-robust and cheap electron donor, triphenylphosphine oxide (TPPO), was successfully adopted to realize *n*-type doping of SnO_2, which was confirmed directly by

electrostatic force microscopy (EFM) and the blue shift of Sn 3d core level in X-ray Photoelectron Spectroscopy (XPS) results. Density functional theory (DFT) calculations were employed to discover the details of charge transfer between TPPO and SnO_2, which reveals that the interaction between TPPO and SnO_2 surface (with or w/o oxygen vacancy) is very strong and electrons are transferred from the R_3P^+-O^- σ-bond mainly to the peripheral tin atoms other than directly interacted tin atoms at the SnO_2 surface. Most importantly, that means the electrons received by the peripheral Sn atoms are delocalized at the surface. To our best knowledge, this phenomenon was reported for the first time by this work. This doping effect accounts for the enhancement of conductivity and the decline of work function of SnO_2, which enlarges the built-in field from 0.01 eV to 0.07 eV and decreases the energy barrier from 0.55 eV to 0.39 eV at the SnO_2/Perovskite interface enabling an increase in the conversion efficiency of PSCs from 19.01% to 20.69%.

Results and Discussion

TPPO is a tetrahedral molecule with three benzenes rings at the three vertices in a plane and the oxygen atom at the other vertex.[28] Expected molecule configuration of TPPO due to linkage between oxygen atoms of TPPO and tin atoms on the surface of SnO_2 nanocrystals is illustrated in Figure 1a. Table S1 and Figure S1 show the typical electronic structure of TPPO molecule calculated by Gaussian 09 software package, with the 6-31+G (d) basis set (BS1) and B3LYP-D3 method,[29, 30] where its lowest unoccupied molecular orbital (LUMO) and highest occupied molecular orbital (HOMO) are ca. -1 eV and ca. -7 eV, respectively. The HOMO of TPPO is much lower than the conduction band minimum (CBM) of SnO_2 (-4.35 eV). According to the routine criterion of *n*-doping, the ionization potential (similar as “HOMO” and valence band maximum “VBM”) of the dopant should be smaller than the electron affinity (similar as “LUMO” and “CBM”) of the host,[2] which results in the ground-state integer electron transfer from the TPPO to SnO_2. The energy level positions of the two materials would thus appear to be unfavorable for the electron transfer. However, this simplified understanding of doping based on ionization

potential (IP) and electron affinity (EA) values of dopant and host does not fully explain the doping process for various organic materials.

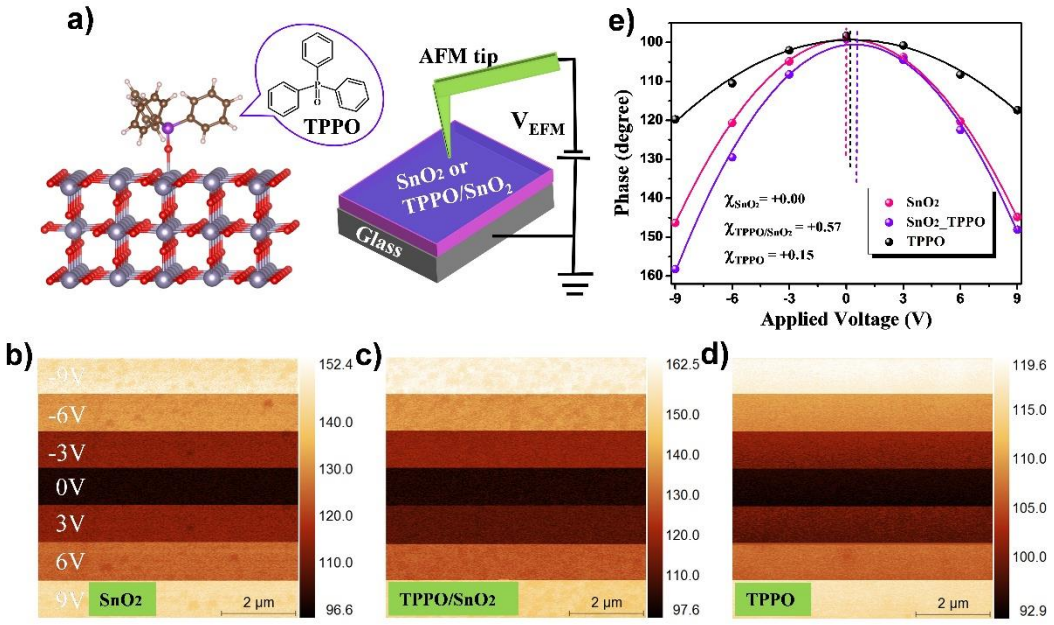

Figure 1. a) The relaxed model of a TPPO molecule absorbed on SnO_2 (110) surface and the EFM measurement. b–d) The phase images under various bias of the bare SnO_2, TPPO doped SnO_2, and TPPO, respectively; e) Plots of the phase as function of applied bias. The solid lines are the corresponding polynomial fittings while the dash lines denote the symmetry axis of the fitting parabola.

Then, we employed EFM to discover whether any charge transfer between the absorbed TPPO molecules and the underlying SnO_2 nanocrystals film occurs. Here it should be noted that all the TPPO coated samples need washing with with chlorobenzene following the same procedure in the device fabrication (Supporting Information). The testing scheme is illustrated in Figure 1a, where the bias voltage (-9V to 9V with an increment of 3V) was applied to the tip allow extraction of the Coulombic force.[31] The phase shift mapping across the whole scan region at different bias voltages are integrated in one image for comparison (Fig. 1b-d). It should be noted here that the size of SnO_2 nanocrystals involved in this work was 3-4 nm and the nanocrystals are dispersed in water.[32] To prepare the standard EFM samples, SnO_2, TPPO and TPPO/ SnO_2 were spin coated on bare insulating glass

substrates. The topographic atomic force microscope (AFM) images of the three EFM samples are shown in Figure S2. The SnO_2 nanocrystal samples show obvious grains morphology while the surface of the TPPO-only sample shows too flat to be discerned. Correspondingly, the phase images in Figure 1b-c also show clear grains and grain boundaries owing to the high space resolution of our EFM. The differences in the phase shift degree of the samples can be easily distinguished. Different from our former report,[13] the positive shifts of the symmetry axis of the fitting parabola in this work indicate positive charge induced at the sample surface (Fig. 1e). The x-values of the symmetric axis of those fitting parabola are 0.00V for SnO_2, 0.15V for TPPO and 0.57V for TPPO/SnO_2, respectively. They are proportional to surface charge density at the surface. For the bare SnO_2 0.00V means very low charge concentration induced. For the TPPO thin layer, a small amount of positive charges can be induced while their concentration of them was obviously augmented for the TPPO modified SnO_2 sample. This phenomenon moves us to learn in-depth about TPPO molecule itself and its interaction with SnO_2. Firstly, this interaction may be origin from the polarized singly σ-bond, R_3P^+-$O^-$of TPPO molecule [33-35] Rationally, the polarized oxygen (O^-) atom with rich electrons is inclined to lose electrons to directly connected tin atoms at the surface, which would lead to positively ionized TPPO molecules and hence accounts for the positive charges detected by EFM (Fig.1).[31]

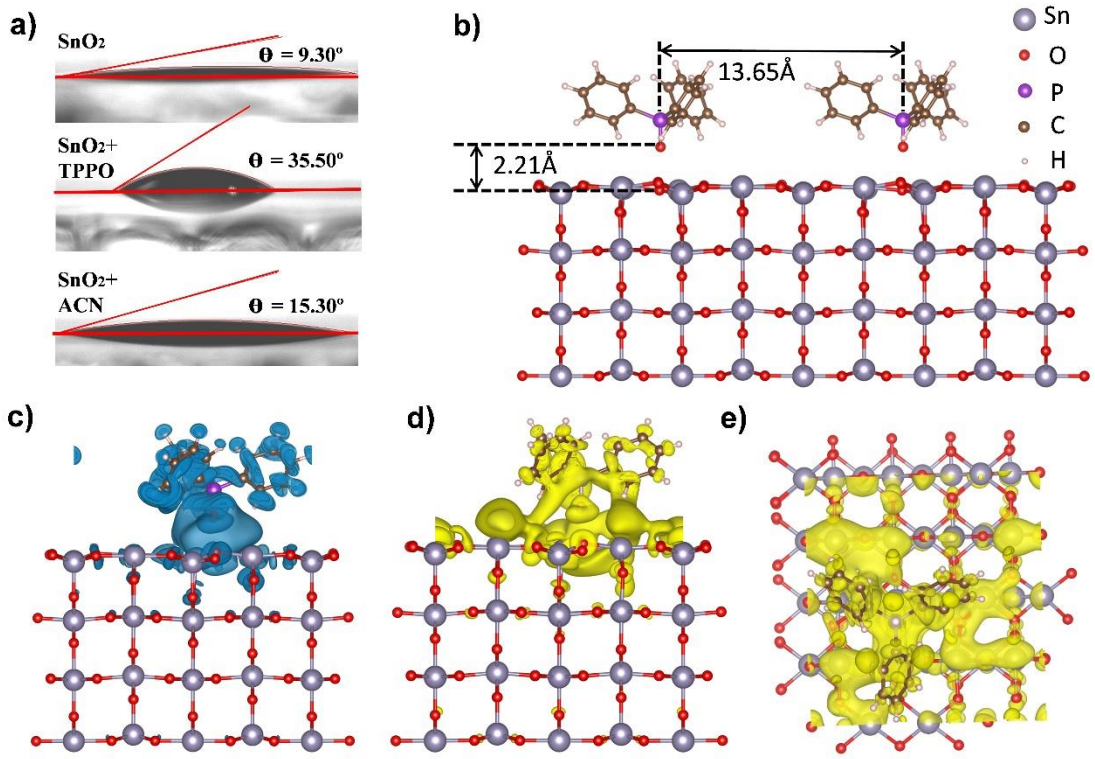

Figure 2. a) Surface contact angles of SnO_2, TPPO doped SnO_2 and SnO_2 treated with acetonitrile on ITO substrates; b) Side-view of the relaxed model of TPPO absorbed SnO_2 (110) surface. Charge density difference (Δρ) of TPPO on SnO_2 (110) surface was calculated at isovalue of 1.2×10^{-4}|e|/Å^3: c) Blue indicate electron depletion and d) yellow indicate electron accumulation; e) Top view of charge density difference (Δρ) of TPPO absorbed on SnO_2 (110), electron gain is indicated by yellow. The different atoms are labeled in panel (b).

To confirm our speculation and gain insight into the experimental results, theoretical calculations were performed by using DFT. As mentioned above, the oxygen atom of TPPO molecule may connect with the Sn atom of SnO_2 nanocrystals at the film surface, which leaves the other three ends of this tetrahedral molecule facing upward, which is tested by the contact angle measurement (Fig. 2a). The contact angle increases obviously after coating a thin layer of TPPO on SnO_2 nanocrystal films. Based on this configuration, a TPPO molecule was put on a 4×2 (110) surface with lattice parameters of 12.97 Å ×13.65 Å (Fig. 2b).[36] Several different adsorption configurations of TPPO molecule on SnO_2 (110) surface with and without oxygen vacancy concentration of 1/112 are considered. The adsorption energy is defined by $E_{ads} = E_{SnO_2+TPPO} - E_{SnO_2} - E_{TPPO}$, where E_{SnO_2+TPPO} is the

total energy of the TPPO molecule adsorbed on SnO_2 (110) surface, E_{SnO_2} is the energy of SnO_2 (110) surface, and E_{TPPO} is the energy of TPPO molecule. The van der Waals (vdW) interactions are also considered. Negative adsorption energies indicate that TPPO molecule adsorbed on SnO_2 (110) surface are stable. According to the definition of E_{ads}, a more negative value of adsorption energy indicates stronger interactions between molecule and SnO_2 surface. The calculated adsorption energies are -1.44 eV for defect-free surface and -1.56 eV for surface with O vacancy. The optimal vertical interlayer-distance between molecule and surface are 2.28 Å for TPPO on perfect surface and 2.21 Å for O vacancy structure (Fig. 2b), respectively. The TPPO molecule adsorption on SnO_2 surface causes a change in the local structure. In addition, the charge density differences ($\Delta\rho = \rho_{SnO_2+TPPO} - \rho_{SnO_2} - \rho_{TPPO}$) of TPPO on SnO_2 (110) surface are calculated to express the interaction between SnO_2 and TPPO molecule (Fig. 2 and Fig. S3). The resulting electron clouds at the interface demonstrate charge redistribution and a strong interaction between SnO_2 and TPPO. The blue could (Fig. 2c) denotes the electron loss from the relative bonds or atoms after the charge redistribution while the yellow (Fig. 2d) means the electron acquired by the relative atoms. Most importantly, besides of the fluctuation of electron cloud of the three benzene rings, it is vital in the conclusion that R_3P^+-O^- bond is mainly responsible for the loss of electrons while the peripheral tin atoms obtain the electrons, which is clearly shown in top view of Figure 2e. This calculation result confirms our speculation that the positive charge induced by the bias voltage of EFM can be attributed to electron loss of R_3P^+-O^- σ bond. Strikingly, as Fig. 2e shows, more received electron clouds spread to peripheral tin atoms other than the directly connected tin atoms in the redistribution. According to Bader charge analysis,[37] the direct connected tin atom does not get electrons from R_3P^+-O^- σ bond. That indicates the electrons received by the peripheral tin atoms at the surface are delocalized. The yield of surface delocalized electron previously reported was attributed to non-stoichiometric states of SnO_{2-x}.[38, 39] As a result of TPPO doping, the number of delocalized electrons on Sn atoms of SnO_2 surface is remarkably augmented after

absorption of TPPO molecules. The doping of TPPO results in the surface electron concentration is 3.9×10^{12} cm^{-2} for the SnO_2 nanocrystals with oxygen vacancies (Fig. 2e), and 5.1×10^{12} cm^{-2} for the defect-free SnO_2 (Fig. S.3b). For comparison, two-dimensional (2D) surface electron concentration of SnO_2 nanoparticles can be estimated to be ~10^{10} cm^{-2}, based on the reported bulk value (~10^{15} cm^{-3}),[40] and extracted by a factor of 2/3 ($n_{2D}=(n_{3D})^{2/3}$))[41] The possible reason for the change in the conductivity of SnO_2 ETL by TPPO doping is the improved conductivity across the grain boundaries doped by TPPO molecules. This is confirmed by the conductive AFM (c-AFM) (Fig. S4). The c-AFM current is enhanced from 66 pA to 260 pA in mean of the scan region after coating of TPPO molecules. The obvious topographic current contrast (Fig. S4b) indicates the coverage divergence of the ionized TPPO molecules penetrating throughout the bulk of SnO_2 nanocrystals film more than just absorbed on the film surface, which will be illustrated below. The surface delocalized electrons would also cause anisotropic dipole polarizability and hence the change of surface electrical field,[38, 42] which is verified by the increase of surface potential measured by Kelvin probe microscopy (Fig. S5).

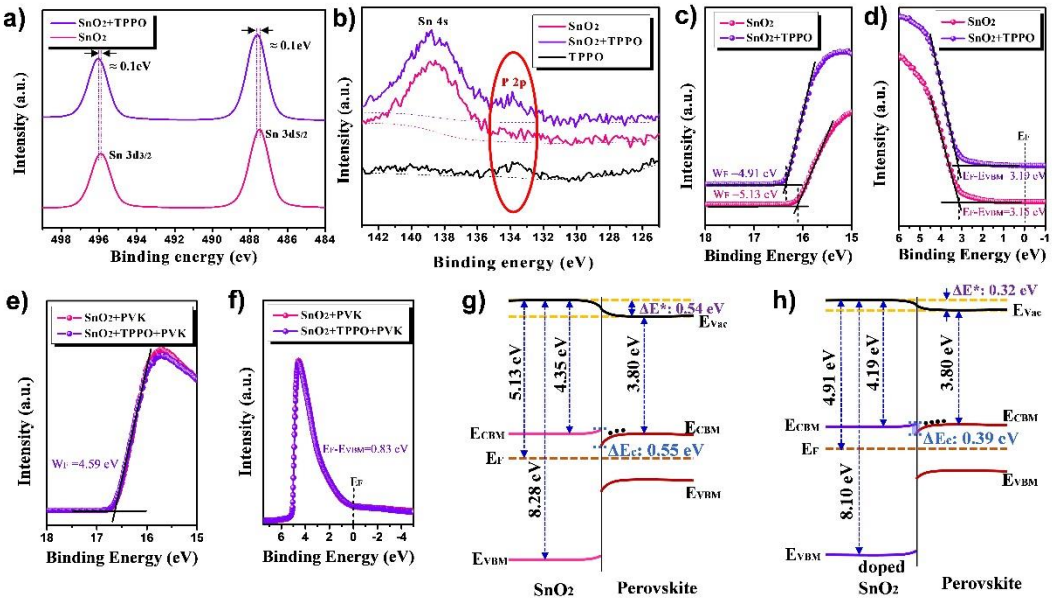

Figure 3. a) XPS core level spectra of Sn 3d on SnO_2 and TPPO doped SnO_2 film; b) The signal of phosphorus circled in red in the XPS spectra of the above three samples; c) and d) The onset and tail of UPS spectra of the bare SnO_2 and TPPO doped SnO_2,

respectively, where their work functions and VBMs can be derived. e) and f) The onset and tail of UPS spectra of CsFAMA perovskite films with 600 nm in thickness deposited on the SnO_2/ITO and TPPO/SnO_2/ITO substrates, respectively, where the differences in work functions and VBMs between each other are negligible; g) and h) Band level diagram of SnO_2/CsFAMA heterojunction before and after doping of TPPO, respectively.

To further confirm electron transfer from TPPO to SnO_2, XPS was utilized to analyze the core-level chemical shift of tin (Fig. 3a-b). Figure 3b examines the existence of TPPO thin layer on the SnO_2 surface via phosphorus element. The blue shift (towards high binding energy) of Sn 3d shown in Figure 3a demonstrates electron transfer to tin atoms at the surface.[5, 6, 11, 36, 38] Thereafter, the work function of SnO_2 surface also shifted from -5.13 eV to -4.91 eV after modification of TPPO as the ultraviolet photoelectron spectroscopy (UPS) results show in Figure 3c, the XPS and UPS results verify the electron transfer from TPPO to SnO_2. The following Kelvin probe measurements show the surface potential of SnO_2 increased from 288 mV to 363 mV after TPPO modification (Fig. S5), which is consistent in conclusion with the UPS results.[43-45]

Figure 3d shows the values of E_F-E_{VBM} of SnO_2 and SnO_2-TPPO. Along with the band gaps derived from the absorption spectra and their corresponding Tauc plots (Fig. S6 a-b), the electronic structures of both SnO_2 and SnO_2-TPPO can be acquired. One information should be noted here that E_{CBM}-E_F decreases after coating the thin layer of TPPO molecules, which indicates that the electron density in the SnO_2 ETLs is enhanced by the surface doping.[1] Very small change in the bandgap value (0.02 eV) obtained from Tauc plots is observed after doping. The UPS and absorption measurements of mixed cation $Cs_{0.05}(FA_{0.85}MA_{0.15})_{0.95}Pb(Br_{0.15}I_{0.85})_3$ perovskite (hereafter CsFAMA) layers on both SnO_2 and SnO_2-TPPO were also obtained as shown in Fig.3e-f and Fig.S6 c-d. The obtained values for E_F, E_{VBM} and E_{CBM} of CsFAMA samples are -4.59 eV, -5.42 eV, and -3.8 eV, respectively. Their Fermi levels remain just 0.02 eV higher than the center of their bandgaps, which can be ascribed to the large thickness (hundreds of nm) of the perovskite layer, so that the perovskite surface is far from the interface of SnO_2/Perovskite.[46] In addition, Figure S7 shows

the topographic scanning electron microscope (SEM) images and X-ray diffraction (XRD) patterns of these perovskite films, which were prepared in the same composition and process as our former report delivered.[18] High quality perovskite films are clearly obtained on both SnO_2 or SnO_2-TPPO, so that any difference in device performance can be attributed to the change in the properties of SnO_2 after TPPO doping. Due to the shift of the work function and the change in the surface electron density of SnO_2 after TPPO doping, the energy band alignment at the interface is expected to be affected by the doping. The energy band level alignments of SnO_2 or SnO_2-TPPO with the perovskite layers deposited on them are shown in Figure 3g-f, respectively. According to the basic theory of band alignment of heterojunctions,[1] the band bending of each material at the SnO_2/Perovskite interface leads to an energy barrier (ΔE_c) at the interface. Band bending can significantly affect charge extraction, collection and recombination in PSCs.[13] A significant difference after TPPO doping can be observed, namely ΔE_c decreases from 0.55 eV to 0.39 eV. This is expected to facilitate electron transfer at the interface and reduce charge accumulation at the interface.

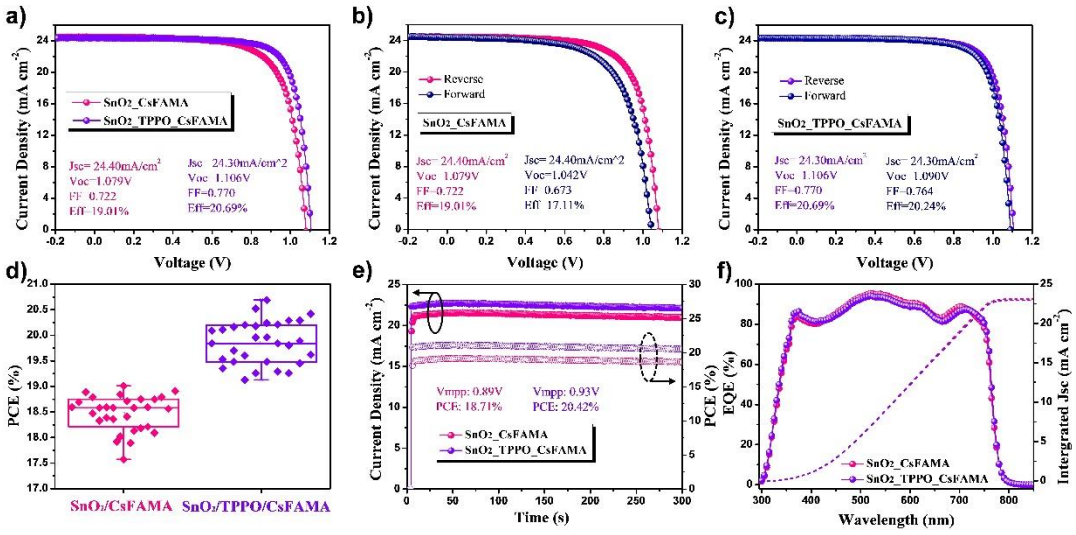

Figure 4. a) *J–V* curves in reverse scan of the optimal CsFAMA PSCs based on SnO_2 and TPPO (1mg/ml)-doped SnO_2 ETLs; b) and c) Hysteresis characteristics of each optimal CsFAMA PSCs based on SnO_2 and TPPO-doped SnO_2 ETLs, respectively; d) Statistics of PCE for the two kinds of devices mentioned above; e) Steady photocurrent and PCE output at a fixed bias voltage of its initial maximal power point

of each champion device; f) EQE spectra and their corresponding integrated Jsc of each champion device.

The surface molecular doping effect in this work was demonstrated in device performance of the typical normal planar PSC structure with a basic configuration of "ITO/SnO_2(-TPPO)/CsFAMA/Spiro-MeOTAD/Au". Due to the performance sensitivity of the molecule layer thickness and coverage,[13, 43, 45] different concentration of TPPO solutions were employed to tune them and to optimize the device performance (Fig. S8). The best device performance was obtained for TPPO concentration of 1 mg/ml. Figure 4a shows the champion cell's *J-V* curves in reverse scan of the bare SnO_2 based (pink) and the SnO_2-TPPO based (purple) devices along with their corresponding parameters. The power conversion efficiency (PCE) is remarkably improved from 19.01% to 20.69%, the open circuit voltage (V_{OC}) is enhanced from 1.079V to 1.106V while the current density (J_{SC}) shows small decrease from 24.40 mA/cm^2 to 24.30 mA/cm^2, after surface doping of TPPO on SnO_2 ETLs. The V_{OC}, J_{SC} and FF statistic data are also summarized in Figure S9 and Table S2. The average value of J_{SC}, however, is increased from 24.27 mA/cm^2 to 24.38 mA/cm^2, while the PCE is increased from 18.59% to 19.84%. It should also be noted that the J_{SC} values of devices on bare SnO_2 exhibit significantly larger standard deviation compared to those on SnO_2-TPPO (0.66 vs. 0.14 mA/cm^2). This indicates improvement in surface quality and uniformity with TPPO doping. Figure 4d shows us the PCE distribution of the two kinds of devices for comparison, which shows the average PCE value was augmented obviously. From the external quantum efficiency (EQE) spectra of each champion device (Fig. 4f), the integrated J_{SC} values are 23.10 mA/cm^2 and 22.95 mA/cm^2 for the SnO_2 and SnO_2-TPPO based champion cells, respectively. Small underestimation of J_{SC} from EQE measurements is common, and it likely originates from the spectral mismatch of the solar simulator and the theoretical AM1.5G spectrum, although the effect of device degradation during transportation to another building for the measurement cannot be excluded. The increase in the V_{OC} can be attributed to the barrier reduction and band alignment at the SnO_2/Perovskite by TPPO modification.[18, 47, 48] The main contribution to the PCE increase comes from

the enhancement of the fill factor (FF) from 0.722 to 0.770. This can be attributed to the optimization of series or shunt resistance of devices owing to the doping of TPPO. To investigate the mechanisms responsible for the observed changes, Electrochemical impedance spectroscopy (EIS) measurements were performed. Figure S10a shows us the Nyquist plots of the devices based on both SnO_2 (pink) and SnO_2-TPPO (purple) ETLs, with their equivalent circuit also shown. From the plots, the value of the high-frequency intercept on the real axis is equal to the series resistance (R_s),[49] the high-frequency component corresponds to the transfer resistance (R_{tr}) and the low-frequency one to the recombination resistance (R_{rec}).[50] From the measurements performed at a forward bias voltage (from 0 to 800 mV) with light illumination (Fig. S10b), the R_s of the SnO_2-TPPO based device is always lower than that of the bare SnO_2 based one. Both devices have low R_s values of several ohms, similar to prvious reports of SnO_2 nanoparticles electron transport layers.[40] The observed trends for R_{tr} are similar to those for the R_s. The recombination resistance, however, increased for SnO_2-TPPO based devices. This indicates lower recombination rate and/or faster extraction of the electrons after TPPO doping, [51] in agreement with the device performance improvements and the reduction of the energy barrier for electron transfer at the interface. To explore the recombination loss in the dark, the dark EIS meausrements with a reverse bias voltage of −700mV were conducted. Drawn from their Nyqiust plots shown in Figure S11, the recombination resistance (R_{rec}) for the TPPO doped SnO_2 based device was 540 kΩ in the dark, which is obviously larger than 330 kΩ for the control one. That demonstrates both the two kinds of devices have very low recombination loss.[52] That is also verified by the dark current examined in the I-V curves of devices (**Fig. S12**). As **Figure S12** shows, the dark current density is as low as 10^{-3} mA/cm^{-2}, which is four-order lower than their photocurrents. That manifests clearly that the dark currents of our devices are very low. Maximum power point tracking (MPPT) was also performed to evaluate the stabilized power output (Fig. 4e),[53] the optimal device yielded a stabilized PCE of 18.71% for the SnO_2 and 20.42% for the TPPO doped SnO_2, which were recorded after 300 s light soaking and are comparable to the PCE obtained from the fresh *J–V* curves.

In addition to the enhancement of PCE, the hysteresis was also suppressed after TPPO doping (Fig. S8a-b). Since the perovskite solar cells commonly exhibit hysteresis, a hysteresis index "H-index" was introduced to quantify the hysteresis degree: H-index = ($PCE_{reverse}$ − $PCE_{forward}$)/$PCE_{reverse}$.[16] H-index decreases remarkably from 9.99% to 2.17% after doping of TPPO, which may be attributed to the change in the energy level alignment at the interface, enhanced electron transfer, and the reduction of charge accumulation at the interface.[54, 55] When the thickness of TPPO molecule rises over the optimal value, the augmented film thickness would definitely increase the electron transport path, and hence retard the electron tansfer and even consume those electrons at the interface. On the other hand, extra or redundant absorbing layers of TPPO molecules may not act that effective doping role for SnO_2 when they are far from its surface, which would form an energy barrier in electrons transport.

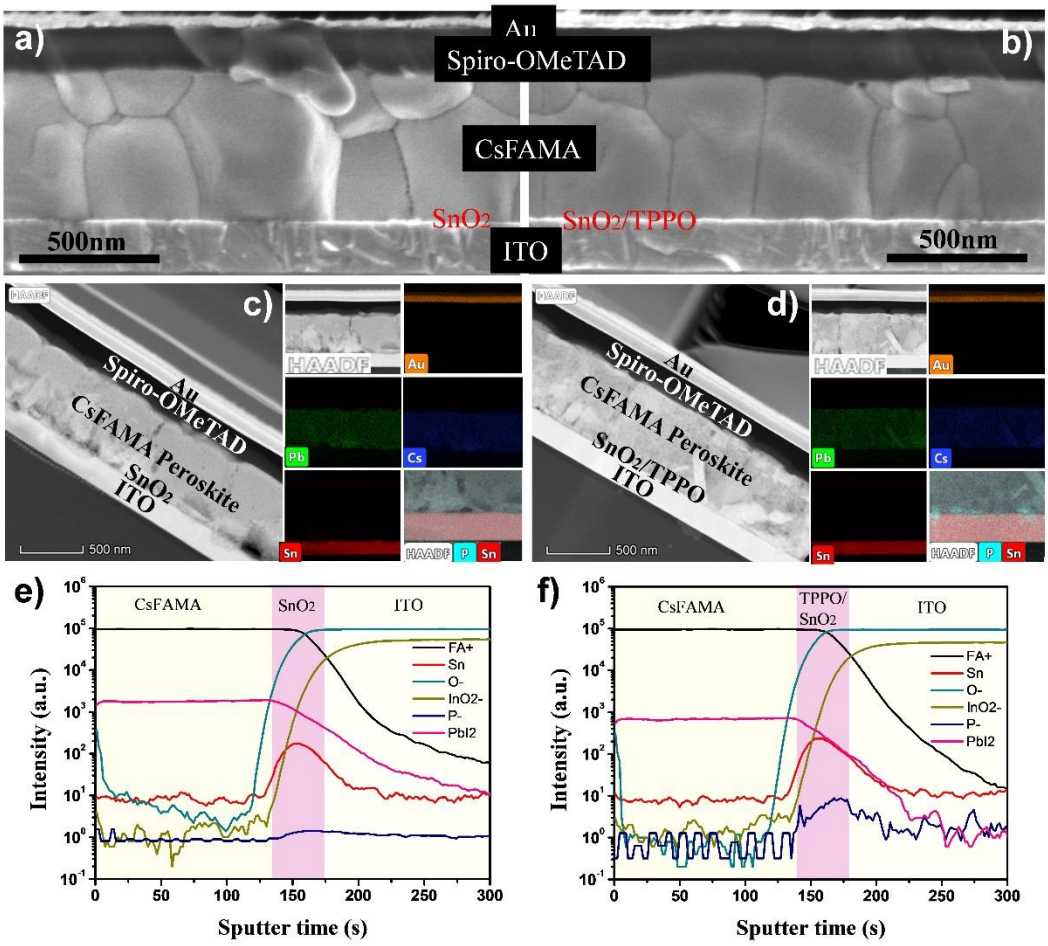

Figure 5. a) and b) Cross-section SEM images of the devices based on SnO_2 and

TPPO doped SnO_2 ETLs, respectively; c) and d) Cross-sectional STEM images and related elemental mappings of the devices based on SnO_2 and TPPO doped SnO_2 ETLs, respectively; e) and f) ToF-SIMS profiles of the ITO/SnO_2/CsFAMA and ITO/SnO_2-TPPO/CsFAMA samples, respectively.

The obtained results clearly demonstrate device performance improvement of CsFAMA PSCs with doping of SnO_2 nanocrystal ETL by TPPO molecules. To further examine the effect of TPPO on the devices and rule out additional differences affecting the device performance, further structural and compositional characterization was performed. Figure 5a and 5b show us the typical cross-section SEM images of devices with SnO_2 and SnO_2-TPPO, respectively. The CsFAMA perovskite films inside are ~600 nm in thickness with compact and large crystalline grains for both kinds of ETLs. The thickness of Spiro-MeOTAD and Au layers are also comparable with each other. Due to the resolution limit, the SnO_2 nanocrystals morphologies cannot be distinguished in these images. Elemental mapping using scanning transmission electron microscopy (STEM) was also performed to explore detailed the cross-section information of our devices at high resolution, especially the element mapping function. Here, the cross-section samples with thickness of ~100 nm were prepared by the focus ion beam (FIB) technique. In Figure 5c-d, the elemental mappings of Pb and Cs prove their uniformity in the CsFAMA layer. The gold electrode layers are also clearly detected. Because the ITO film also contains tin, it's difficult to specify the SnO_2 nanocrystals from the ITO electrode film in these elemental mapping. However, tiny amount of phosphorus was clearly detected in the cross section of SnO_2-TPPO based devices (Fig. 5d). This result was also confirmed by the depth profile of phosphorus concentration characterized by time-of-flight secondary ions mass spectroscopy (ToF-SIMS). Figure 5e-f list depth profile concentration of some key elements involved in the device structure, where the pink band indicates the approximate position of the SnO_2 ETL layer. The presence of phosphorus (dark blue line in Fig. 5e and 5f) can be clearly observed throughout the SnO_2:TPPO, which indicates that TPPO molecules may penetrate throughout the SnO_2 layer and be absorbed at the grain boundaries. In addition, we can observe a difference in CsFAMA ion profiles, which may indicate possible reduction in the ion

diffusion, which is consistent with grain boundary passivation in SnO_2 ETL and may also contribute to the reduced hysteresis.

Conclusion

In summary, we discovered a novel surface molecular doping mechanism in organic/inorganic hybrid electronics. It seems impossible in electron transfer from TPPO molecule to SnO_2 because the ionization potential of TPPO (ca. -8 eV) is much deeper than the CBM of SnO_2 (-4.35 eV). However, the electron transfer was realized successfully and verified directly by EFM, and confirmed by the shift in Sn 3d core level of XPS results to higher energy. The DFT simulation reveals that the interaction between TPPO and SnO_2 surface (with or w/o oxygen vacancy) is very strong and the electrons are transferred from the R_3P^+-O^- σ-bond mainly to the peripheral tin atoms other than directly connected tin atoms at the SnO_2 surface, which results in the presence of delocalized electrons at the surface, and consequently increased conductivity and decreased work function. This in turn results in an increase of the built-in field from 0.01 eV to 0.07 eV, while the energy barrier at the SnO_2/Perovskite interface decreases from 0.55 eV to 0.39 eV. The molecular doping by TPPO enables an increase in PCE from 19.01% to 20.69%, while the hysteresis index is significantly reduced from 9.99 % to 2.17%. The improvements in the device performance can be attributed to faster electron extraction and lower recombination rate. This comprehensive work broadens the scope of rising organic/inorganic hybrid electronics and provides deeper insight into the mechanisms of surface molecular doping.

Acknowledgements

We thank Prof. Hongtao He from the Department of Physics for valuable discussion on surface delocalized electrons. We also thank Mr. Huqiang Yi from the Department of Materials Science and Engineering and the Materials Characterization and Preparation Center (MCPC) of SUSTech for some characterizations in this work. This work is supported by the National Natural Science Foundation of China (NSFC)

(Nos. 61775091, 11474145), National Key Research Project MOST (No. 2016YFA0202400), the Shenzhen Key Laboratory Project (No. ZDSYS201602261933302) and Natural Science Foundation of Shenzhen Innovation Committee (Nos. JCYJ20150529152146471, JCYJ20160530184523244 JCYJ20170818141216288 JCYJ20170817105007999, JCYJ20170817104736009), and H.-F. Li acknowledges the financial support from the Science and Technology Development Fund from Macau SAR (FDCT-064/2016/A2 and FDCT-028/2017/A1). Financial support from the Seed Funding for Strategic Interdisciplinary Research Scheme of the University of Hong Kong and RGC GRF grants 15204515 and 15246816 are acknowledged.

Contributions

B. Tu designed and finished all the experiments of this work, as well as the analysis of the data collected. DFT calculations on the interaction between TPPO and SnO_2 were accomplished by Y.F. Shao. W. Chen directed the fabrication and optimization of PSCs involved. Multifunction AFM tests were conducted with some analysis by Y.H. Wu. X. Li contributed to the Gaussian calculations for TPPO molecule. FIB and STEM tests were under help of Y.L. He and J.X. Li. Dr. F.Z. Liu performed TOF-SIMS measurements and Z. Zhang helped deal with the EIS results. Y. Lin, X.Q. Lan and L.M. Xu contributed themselves to the characterizations of some materials and devices involved. Prof. X.Q. Shi directed the calculation process of DFT, afforded valuable results discussion and revised the manuscript. Prof. H.F. Li cultivated B. Tu in both experiments and results analysis along with revision of this paper. Prof. A.M. Ng, Prof. L.W. Chung and Prof. A.B. Djurisic took part in the valuable mechanism discussion of some results and revised the manuscript. Prof. Z.B. He conceived the idea, directed the process and wrote the manuscript.

References:

[1] S. M Sze, *Physics of Semiconductor Devices. New York*, Vol. 1, **1981**.
[2] B. Lussem, C. M. Keum, D. Kasemann, B. Naab, Z. Bao, K. Leo, *Chem. Rev.* **2016**, 116, 13714.
[3] H. Mendez, G. Heimel, S. Winkler, J. Frisch, A. Opitz, K. Sauer, B. Wegner, M. Oehzelt, C. Rothel, S. Duhm, D. Tobbens, N. Koch, I. Salzmann, *Nat. Commun.* **2015**, 6, 8560.
[4] I. Salzmann, G. Heimel, M. Oehzelt, S. Winkler, N. Koch, *Acc Chem Res* **2016**, 49, 370.
[5] K. J. Rietwyk, Y. Smets, M. Bashouti, S. H. Christiansen, A. Schenk, A. Tadich, M. T. Edmonds, J. Ristein, L. Ley, C. I. Pakes, *Phys. Rev. Lett.* **2014**, 112, 155502.
[6] A. Tarasov, S. Zhang, M.-Y. Tsai, P. M. Campbell, S. Graham, S. Barlow, S. R. Marder, E. M. Vogel, *Adv. Mater.* **2015**, 27, 1175.
[7] A. R. Kirmani, A. Kiani, M. M. Said, O. Voznyy, N. Wehbe, G. Walters, S. Barlow, E. H. Sargent, S. R. Marder, A. Amassian, *ACS Energy Lett.* **2016**, 1, 922.
[8] J. I. Martinez, F. Flores, J. Ortega, S. Rangan, C. Ruggieri, R. Bartynski, *J. Phys. Chem. C* **2015**, 119, 22086.
[9] R. Schlesinger, F. Bianchi, S. Blumstengel, C. Christodoulou, R. Ovsyannikov, B. Kobin, K. Moudgil, S. Barlow, S. Hecht, S. R. Marder, F. Henneberger, N. Koch, *Nat. Commun.* **2015**, 6, 6754.
[10] S. P. Schiessl, H. Faber, Y. H. Lin, S. Rossbauer, Q. Wang, K. Zhao, A. Amassian, J. Zaumseil, T. D. Anthopoulos, *Adv Mater* **2016**, 28, 3952.
[11] Y. H. Kim, D. G. Kim, R. D. Maduwu, H. C. Jin, D. K. Moon, J. H. Kim, *Solar RRL* **2018**, *2*, 1800086.
[12] T. Schultz, J. Niederhausen, R. Schlesinger, S. Sadofev, N. Koch, *J. Appl. Phys.* **2018**, 123, 245501.
[13] W. Chen, Y. Zhou, L. Wang, Y. Wu, B. Tu, B. Yu, F. Liu, H. W. Tam, G. Wang, A. B. Djurisic, L. Huang, Z. He, *Adv Mater* **2018**, 30, 1800515.
[14] W. J. Ke, G. J. Fang, Q. Liu, L. B. Xiong, P. L. Qin, H. Tao, J. Wang, H. W. Lei, B. R. Li, J. W. Wan, G. Yang, Y. F. Yan, *J. Am. Chem. Soc.* **2015**, 137, 6730.
[15] Q. Jiang, X. Zhang, J. You, *Small* **2018**, 14, 1801154.
[16] Q. Jiang, Z. Chu, P. Wang, X. Yang, H. Liu, Y. Wang, Z. Yin, J. Wu, X. Zhang, J. You, *Adv. Mater.* **2017**, 29, 1703852.
[17] NREL, *https://www.nrel.gov/pv/assets/images/efficiency-chart.png* Acessed in September of **2018**.
[18] G. Yang, C. Chen, F. Yao, Z. Chen, Q. Zhang, X. Zheng, J. Ma, H. Lei, P. Qin, L. Xiong, W. Ke, G. Li, Y. Yan, G. Fang, *Adv. Mater.* **2018**, 30, 1706023.
[19] J. Xie, K. Huang, X. Yu, Z. Yang, K. Xiao, Y. Qiang, X. Zhu, L. Xu, P. Wang, C. Cui, D. Yang, *ACS Nano* **2017**, 11, 9176.
[20] W. Q. Wu, D. Chen, Y. B. Cheng, R. A. Caruso, *Solar RRL*. **2017**, 1, 1700117.
[21] C. Wang, D. Zhao, C. R. Grice, W. Liao, Y. Yu, A. Cimaroli, N. Shrestha, P. J. Roland, J. Chen, Z. Yu, P. Liu, N. Cheng, R. J. Ellingson, X. Zhao, Y. Yan, *J. Mater. Chem. A* **2016**, 4, 12080.
[22] X. Liu, K.-W. Tsai, Z. Zhu, Y. Sun, C.-C. Chueh, A. K. Y. Jen, *Adv. Mater. Interfac.* **2016**, 3, 1600122.

[23] W. Ke, D. Zhao, C. Xiao, C. Wang, A. J. Cimaroli, C. R. Grice, M. Yang, Z. Li, C.-S. Jiang, M. Al-Jassim, K. Zhu, M. G. Kanatzidis, G. Fang, Y. Yan, *J. Mater. Chem. A* **2016**, 4, 14276.
[24] H. S. Rao, B. X. Chen, W. G. Li, Y. F. Xu, H. Y. Chen, D. B. Kuang, C. Y. Su, *Adv. Funct. Mater.* **2015**, 25, 7200.
[25] Y. Li, J. Zhu, Y. Huang, F. Liu, M. Lv, S. Chen, L. Hu, J. Tang, J. Yao, S. Dai, *RSC Adv.* **2015**, 5, 28424.
[26] K. Choi, J. Lee, H. I. Kim, C. W. Park, G.-W. Kim, H. Choi, S. Park, S. A. Park, T. Park, *Energ. Environ. Sci.* **2018**, DOI: 10.1039/C8EE02242A.
[27] D. Yang, R. Yang, K. Wang, C. Wu, X. Zhu, J. Feng, X. Ren, G. Fang, S. Priya, S. F. Liu, *Nat. Commun.* **2018**, 9, 3239.
[28] S. A. L. A., *Acta Cryst.* **1987**, C43, 1233.
[29] A. D. Becke, *J. Chem. Phys.* **1993**, 98, 5648.
[30] A. D. Becke, *Phy. Rev. A* **1988**, 38, 3098.
[31] S. E. Yalcin, J. A. Labastide, D. L. Sowle, M. D. Barnes, *Nano Lett.* **2011**, 11, 4425.
[32] Q. Jiang, L. Q. Zhang, H. L. Wang, X. L. Yang, J. H. Meng, H. Liu, Z. G. Yin, J. L. Wu, X. W. Zhang, J. B. You, *Nat. Energy* **2017**, 2, 1.
[33] J. A. M.-G. Dobado, H. Molina, J. M. Sundberg, M. R., *J. Am. Chem. Soc.* **1998**, 120, 8461.
[34] D. B. Chesnut, *J. Am. Chem. Soc.* **1998**, 120, 10504.
[35] D. L. E. Bryce, K. Wasylishen R. E., *Inorg. Chem.* **2003**, 42, 5085.
[36] M. Batzill, U. Diebold, *Prog. Surf. Sci.* **2005**, 79, 47.
[37] S. Grimme, J. Antony, S. Ehrlich, H. Krieg, *J. Chem. Phys.* **2010**, 132, 154104.
[38] Y. G. P. Kang, H. G. Kim, H. J. Kim, Y. H. Oh, B. Y. Kim, B. Y. Kim, D. H. Seo D. S., *Opt. Express* **2010**, 18, 21594.
[39] X. Z. Xu, J. Wang X., *J. Am. Chem. Soc.* **2008**, 130, 12527.
[40] L. Xiong, M. Qin, C. Chen, J. Wen, G. Yang, Y. Guo, J. Ma, Q. Zhang, P. Qin, S. Li, G. Fang, *Adv. Funct. Mater.* **2018**, 28, 1706276.
[41] C. Kittel, D. F. Holcomb, *American Journal of Physics* **1967**, 35, 547.
[42] M. MedveĎ, P. W. Fowler, J. M. Hutson, *Mol. Phys.* **2000**, 98, 453.
[43] W. Chen, Y. Zhu, Y. Yu, L. Xu, G. Zhang, Z. He, *Chem. Mater.* **2016**, 28, 4879.
[44] W. Chen, G. N. Zhang, L. M. Xu, R. Gu, Z. H. Xu, H. J. Wang, Z. B. He, *Mater Today Energy* **2016**, 1-2, 1.
[45] W. Chen, L. Xu, X. Feng, J. Jie, Z. He, *Adv Mater* **2017**, 29, 1603923.
[46] K. Lu, Y. Lei, R. Qi, J. Liu, X. Yang, Z. Jia, R. Liu, Y. Xiang, Z. Zheng, *J. Mater. Chem. A* **2017**, 5, 25211.
[47] D. Yang, X. Zhou, R. Yang, Z. Yang, W. Yu, X. Wang, C. Li, S. Liu, R. P. H. Chang, *Energy Environ. Sci.* **2016**, 9, 3071.
[48] J. P. Correa Baena, L. Steier, W. Tress, M. Saliba, S. Neutzner, T. Matsui, F. Giordano, T. J. Jacobsson, A. R. Srimath Kandada, S. M. Zakeeruddin, A. Petrozza, A. Abate, M. K. Nazeeruddin, M. Grätzel, A. Hagfeldt, *Energy Environ. Sci.* **2015**, 8, 2928.
[49] A. Todinova, J. Idigoras, M. Salado, S. Kazim, J. A. Anta, *J. Phys. Chem. Lett.*

2015, 6, 3923.
[50] D. Yang, R. Yang, J. Zhang, Z. Yang, S. Liu, C. Li, *Energy Environ. Sci.* **2015**, 8, 3208.
[51] J. Zhang, C. Shi, J. Chen, Y. Wang, M. Li, *J. Solid State Chem.* **2016**, 238, 223.
[52] M. M. Byranvand, T. Kim, S. Song, G. Kang, S. U. Ryu, T. Park, *Adv. Energy. Mater.* **2018**, 8, 1702235.
[53] S. Song, B. J. Moon, M. T. Hörantner, J. Lim, G. Kang, M. Park, J. Y. Kim, H. J. Snaith, T. Park, *Nano Energy* **2016**, 28, 269.
[54] M. F. Ayguler, A. G. Hufnagel, P. Rieder, M. Wussler, W. Jaegermann, T. Bein, V. Dyakonov, M. L. Petrus, A. Baumann, P. Docampo, *ACS Appl. Mater. Inter.* **2018**, 10, 11414.
[55] G. Yang, C. L. Wang, H. W. Lei, X. L. Zheng, P. L. Qin, L. B. Xiong, X. Z. Zhao, Y. F. Yan, G. J. Fang, *J. Mater. Chem. A* **2017**, 5, 1658.